Loop 2 of *Limulus* Myosin III Is Phosphorylated by Protein Kinase A and Autophosphorylation†

Karen Kempler,‡ Judit Tóth,§,|| Roxanne Yamashita,§ Gretchen Mapel,‡ Kimberly Robinson,‡ Helene Cardasis,⊥,# Stanley Stevens,⊥ James R. Sellers,§ and Barbara-Anne Battelle*,‡

Whitney Laboratory for Marine Bioscience and the Department of Neuroscience, University of Florida, St. Augustine, Florida 32080, Proteomics Core of the ICBR and Department of Chemistry, University of Florida, Gainesville, Florida 32010, Department of Biochemistry, Eötvös Loránd University, Pázmány P.s. 1/c., Budapest 1117, Hungary, and Laboratory of Molecular Physiology, NHLBI, National Institutes of Health, Bethesda, Maryland 20892-1762

Received October 10, 2006; Revised Manuscript Received January 25, 2007

ABSTRACT: Little is known about the functions of class III unconventional myosins although, with an N-terminal kinase domain, they are potentially both signaling and motor proteins. *Limulus* myosin III is particularly interesting because it is a phosphoprotein abundant in photoreceptors that becomes more heavily phosphorylated at night by protein kinase A. This enhanced nighttime phosphorylation occurs in response to signals from an endogenous circadian clock and correlates with dramatic changes in photoreceptor structure and function. We seek to understand the role of *Limulus* myosin III and its phosphorylation in photoreceptors. Here we determined the sites that become phosphorylated in *Limulus* myosin III and investigated its kinase, actin binding, and myosin ATPase activities. We show that *Limulus* myosin III exhibits kinase activity and that a major site for both protein kinase A and autophosphorylation is located within loop 2 of the myosin domain, an important actin binding region. We also identify the phosphorylation of an additional protein kinase A and autophosphorylation site near loop 2, and a predicted phosphorylation site within loop 2. We show that the kinase domain of *Limulus* myosin III shares some pharmacological properties with protein kinase A, and that it is a potential opsin kinase. Finally, we demonstrate that *Limulus* myosin III binds actin but lacks ATPase activity. We conclude that *Limulus* myosin III is an actin-binding and signaling protein and speculate that interactions between actin and *Limulus* myosin III are regulated by both second messenger mediated phosphorylation and autophosphorylation of its myosin domain within and near loop 2.

Class III unconventional myosins are unique members of the myosin superfamily. In addition to the motor domain, neck region, and tail domain typically found in unconventional myosins, class III myosins have a kinase domain at their N-terminus (*1*). Thus, class III myosins may exhibit both signaling and motor functions, yet little is known about their biochemical properties or their roles in cellular processes.

In *Drosophila* and *Limulus*, species in which class III myosins were first identified, myosin III (MYO3)[1] expression appears photoreceptor specific (*2*, *3*). More recently, class III myosins have been detected in the photoreceptors of diverse invertebrate and vertebrate species including humans (*4*−*9*). These findings suggest that MYO3s are particularly important for photoreceptors, although their functions in the photoreceptors of invertebrates and vertebrates are probably different. In *Limulus* and *Drosophila* photoreceptors, MYO3s concentrate at the actin-rich photosensitive membrane or rhabdom (*3*, *10*). *Drosophila* MYO3 has been implicated in diverse processes including photoreceptor survival (*2*), the termination (*11*) and modulation (*12*) of the photoresponse, calmodulin localization (*13*), pigment migration (*14*), and the translocation of $G_q\alpha$ and visual arrestin from the cytoplasm to the rhabdom (*15*, *16*), although the last observation remains controversial (*17*). In the photoreceptors of vertebrates, MYO3s do not concentrate over the photosensitive outer segment. Rather, they are detected in photoreceptor inner segments in humans and mice (*8*, *9*), and

† Supported by NSF Grants (IBN and IOB) to B.-A.B., an NSF Research Experience for Undergraduates Site grant to the Whitney Laboratory, the Intramural program of the NHLBI, NIH, and the University of Florida's ICBR Proteomics Core Facility.

* Corresponding author. Mailing address: Whitney Laboratory for Marine Bioscience, University of Florida, 9505 Ocean Shore Blvd., St. Augustine, FL 32080. Tel: 904-461-4022. Fax: 904-461-4008. E-mail: Battelle@whitney.ufl.edu.

‡ Whitney Laboratory for Marine Bioscience and the Department of Neuroscience, University of Florida.

§ National Institutes of Health.

|| Eötvös Loránd University.

⊥ Proteomics Core of the ICBR, University of Florida.

Department of Chemistry, University of Florida.

[1] Abbreviations: CaM PK II, calcium calmodulin-dependent protein kinase II; hMYO3, human myosin III; ICBR, Interdisciplinary Center for Biotechnology Research; IDA, information-dependent acquisition; LC, liquid chromatography; LE, lateral eye; LON, lateral optic nerve; LpMYO3, *Limulus* myosin III; LR, *Limulus* Ringer, MALDI, matrix-assisted laser desorption/ionization; MS, mass spectrometric; MYO3, myosin III; NINAC, neither inactivation nor afterpotential C; PKA, cyclic AMP-dependent protein kinase; PKC, protein kinase C; PKI, autoinhibitory peptide for PKA; qTOFMS, quadrupole time-of-flight mass spectrometry; rp, reverse phase; rLpMYO3, recombinant *Limulus* myosin III; S1, myosin subfragment 1; SDS PAGE, SDS polyacrylamide gel electrophoresis; TFA, trifluoroacetic acid; 2D, two-dimensional.

10.1021/bi062112u CCC: $37.00
Published on Web 03/17/2007

also in the actin-rich calycal processes in fish (*7*). A class III myosin is also expressed in the cochlea of mice (*18*) where the protein localizes to the tips of the hair cells (*19*), and a mutation in a human MYO3 has been implicated in progressive hearing loss (*18*).

Limulus myosin III (LpMYO3), the focus of this study, is interesting because it is a circadian clock regulated phosphoprotein that shows enhanced phosphorylation at night (*20*, *21*). Furthermore, the nighttime increase in its phosphorylation correlates with dramatic and diverse changes in retinal structure and function that enhance retinal sensitivity and responsiveness to light (*22*) and prime photoreceptors for light-triggered processes the next day (*22*−*25*). The clock-driven phosphorylation of LpMYO3 at night is mediated by cyclic AMP-dependent protein kinase (PKA) (*20*, *21*). Our goal is to understand the role of LpMYO3 in photoreceptors and the role of its phosphorylation in circadian changes in vision.

Some functions of LpMYO3 have been predicted from its sequence (*3*, accession # AF062089), but few have been tested directly. LpMYO3 has one IQ motif suggesting it binds calmodulin, and the sequence of its N-terminus suggests it is a kinase. It has a myosin motor-like domain (here referred to as the myosin domain) based on sequence similarity with other myosins; therefore it is predicted to bind actin. However, the sequence of the conserved catalytic site in the myosin domain strongly indicates that it may lack the ability to hydrolyze ATP. In particular, it lacks a salt bridge known from studies of other myosins to be critical for ATP hydrolysis (*26*, *27* and Discussion). Its myosin domain also contains three predicted PKA phosphorylation sites which may be the clock-regulated phosphorylation sites.

In a previous study (*3*) we showed that endogenous LpMYO3 in soluble extracts of *Limulus* lateral eye (LE) binds to calmodulin sepharose in the absence and not in the presence of Ca^{++}, but that it failed to bind calmodulin in calmodulin overlay assays. These observations could be interpreted to mean that LpMYO3 binds to calmodulin indirectly or that its affinity for calmodulin is low. We also showed that LpMYO3 can be phosphorylated by PKA within its myosin domain, but the exact sites of phosphorylation were not identified nor did we determine whether the myosin domain was the only target for phosphorylation.

Here we extend our investigations of LpMYO3 phosphorylation and function and show that all PKA phosphorylation sites are located within the myosin domain and that the major site phosphorylated by PKA in both expressed and endogenous LpMYO3 is located within loop 2 of the myosin domain. We also identify a second PKA phosphorylation site on the N-terminal side of loop 2 and an additional phosphorylated site within loop 2 that is a predicted PKC site. We show that LpMYO3 expresses PKA-like kinase activity, and that it undergoes intermolecular autophosphorylation at the same sites phosphorylated by PKA. Finally, we show that LpMYO3 can bind to actin but lacks ATPase activity. Thus, LpMYO3 is probably not a motor. Our findings lead us to propose that interactions between LpMYO3 and actin are modulated by second messenger mediated phosphorylation and autophosphorylation within and near loop 2 of the myosin domain.

EXPERIMENTAL PROCEDURES

Animals and Standard Reagents. Adult *Limulus* were collected and maintained as described previously (*28*). Unless otherwise specified, reagents were obtained from either Sigma-Aldrich or Fisher Scientific.

Baculovirus Transfer Vector Construction and Expression and Purification of Recombinant LpMYO3 (rLpMYO3). Procedures were modified from those described by Wang et al. (*29*). The entire open reading frame of *Lpmyo3* (Accession # AF062089) was obtained by PCR amplification of a full-length lambda cDNA clone of *Lpmyo3* (*3*). The 5′ PCR primer used to amplify cDNA encoding full-length LpMYO3 (nucleotides 1−3042) and cDNA encoding LpMYO3 lacking the IQ and tail domains (ΔIQ LpMYO3 nucleotides 1−2982) contained a *Bgl*II restriction site and a Kozak sequence. The 3′ primer contained sequences encoding a FLAG tag (DYKDDDK) followed by a stop codon and an *Xba*I restriction site. cDNA encoding LpMYO3 that lacks the kinase domain (Δkinase LpMYO3 nucleotides 865−3042) was similarly obtained, except the 5′ primer encoded an initiation methionine in addition to sequences for the *Bgl*II restriction site and Kozak sequence. All products were verified by sequencing in both directions and subcloned into the baculovirus transfer vector pVL1392 (Invitrogen).

All of the myosin constructs were expressed in the baculovirus/sf9 system; full-length and Δkinase LpMYO3 were expressed together with *Drosophila* calmodulin (The viral construct was a gift from Craig Montell). Infected cells were harvested by sedimentation after 48 h to 96 h of growth; the pellet was washed twice with phosphate-buffered saline and either quick-frozen and stored in liquid nitrogen or processed immediately. rLpMYO3 was purified from the sf9 cells as described by Wang et al. (*29*) except that the protein was eluted from the FLAG affinity column with FLAG peptide in buffer containing 0.5 M NaCl.

Fractions (0.5 mL) were collected, an aliquot of each was subjected to SDS PAGE (*30*), and the gels were stained with Coomassie Blue. The concentration of expressed LpMYO3 in each fraction was determined from scans of Coomassie Blue staining intensities quantified by ImageQuant relative to the staining intensities of protein standards (trypsin inhibitor or β galactosidase) processed on the same gels. In some cases the expressed protein was concentrated by Q-Sepharose ion exchange chromatography (*29*). Recombinant protein was stored on ice in buffer containing 0.5 M NaCl or quick-frozen as droplets in liquid nitrogen. Frozen droplets (20 μL) were stored frozen in liquid nitrogen. In some cases 1 μM calmodulin prepared from bovine testes (*31*) was added to all buffers used during purification in an effort to increase protein stability.

Expression in Escherichia coli of a Portion of the Myosin Domain Containing Loop 2 and All Predicted PKA Phosphorylation Sites. cDNA encoding the region of the myosin domain of LpMYO3 that includes loop 2 and all three predicted PKA sites (from N^{781} to D^{940}) (Figure 5) was amplified by PCR. The 5′ and 3′ primers included an *Nde*I and a *Hin*dIII restriction site, respectively, for eventual insertion into pET 28a plasmid (Invitrogen) and expression as a His-tagged fusion protein in BL21(Star)DE3 *E. coli* cells (Invitrogen). The PCR product was cloned into pCR 4-TOPO (Invitrogen), and the wild-type sequence was verified by

sequencing in both directions. Four mutants of the wild-type sequence were produced using the QuikChange Site-Directed Mutagenesis Kit (Stratagene). Each of the three mutants contained one of the three predicted PKA phosphorylation sites, S^{796}, S^{846} or S^{926}; the other two sites were mutated to alanines. In the fourth mutant, all three predicted PKA phosphorylation sites were mutated to alanines. Successful mutagenesis was confirmed by direct sequencing. The wild-type and mutant polypeptides were expressed as insoluble proteins; therefore they were extracted in 6 M urea and purified in 6 M urea with standard Ni chelation chromatography (His-Bind resin, Novagen). Affinity purified proteins were fractionated by SDS PAGE, and the protein concentration of each was determined by its Coomassie Blue staining intensity as described above. Prior to use as substrates for phosphorylation by rLpMYO3, purified polypeptides were dialyzed overnight against Tris buffer at pH 7.5 containing 3 M urea.

Phosphorylation Assays. The reaction mixture for rLpMYO3 autophosphorylation and for the phosphorylation of other substrates by rLpMYO3 contained 15 mM MOPS at pH 7.3, 15 mM $MgCl_2$, 1.5 mM EGTA, 300 mM NaCl, 4.5 mM NaN_3, protease inhibitors as described by Edwards and Battelle (*20*), and 150 μM ATP containing 25 μCi of [γ^{32}P] ATP (Perkin-Elmer, Boston, MA, 10 mCi/mL) in a final volume of 50 μL. Unless otherwise specified, the concentration of rLpMYO3 in the reaction was roughly 0.4 μM. Preliminary studies established that the rate of autophosphorylation was maximum in the presence of 150 μM ATP and linear for at least 3 h at 30 °C. The same conditions were used for PKA phosphorylation of rLpMYO3 except that 8 units of the catalytic subunit of PKA (Sigma) were added to the reaction mixture.

Protein phosphorylation assays were stopped by the addition of SDS sample buffer (*30*) and sonication. Samples were separated by SDS PAGE, and protein phosphorylation was detected as phosphorimages (Phosphorimager SI, Amersham) of dried, Coomassie Blue-stained gels. Phosphorylation was quantified with ImageQuant software. Incorporation of phosphate into protein was normalized to protein concentration as determined from scans of the Coomassie Blue stains also quantified using ImageQuant as described above using trypsin inhibitor and β galactosidase as standards. Peptide phosphorylation was assayed with a phosphocellulose binding assay (*32*).

Endogenous LpMYO3 in homogenates of LON was phosphorylated for 1 h at 30 °C in a final volume of 50 μL containing the reaction buffer described above, 8 units of the catalytic subunit of PKA and 25 μCi of [γ^{32}P] ATP in a final concentration of 30 μM ATP. LONs were homogenized in reaction buffer plus protease inhibitors as described above (5 μL/mg tissue wet weight). For experiments in which endogenous LpMYO3 was phosphorylated in intact, dark-adapted ventral photoreceptors, ventral roots from four animals were preincubated overnight in the dark at 15 °C in 1 mL of organ culture medium (*33*), and all subsequent manipulations occurred in the dark or under infrared illumination. Cells were rinsed four times with 1 mL of *Limulus* Ringer (LR) plus dextrose (*34*), and incubated for 1.5 h at room temperature in 100 μL of LR plus dextrose containing 3 μCi/μL ^{32}P-labeled orthophosphate (MP Biomedicals). Forskolin was then added at a final concentration of 10 μM to activate adenylyl cyclase and the cAMP cascade (*35*) and the incubation continued for 30 min at room temperature. The incubation was stopped with the addition of SDS sample buffer and sonication.

Assays of rLpMYO3 phosphorylation in sf9 cells were performed with attached cultures of 2×10^6 uninfected sf9 control cells and similar cultures of cells infected with viruses containing inserts encoding full-length rLpMYO3 and calmodulin. Cells were incubated overnight in phosphate-free medium (*36*) containing 100 μCi $^{32}PO_4$, scraped from the plates, collected by centrifugation, and processed as described above to purify rLpMYO3. Proteins in total cell homogenates and in the aliquot eluted from the FLAG affinity column with FLAG peptide were separated by SDS PAGE and blotted to nitrocellulose membrane (NitroBind, Osmonics, Inc.). The blots were immunostained for LpMYO3 (*37*) and then analyzed for phosphoproteins as described below.

Substrates. Peptides we tested as substrates for rLpMYO3 are known substrates for other kinases: PKA (S^{21} of PKI 14-22, Gly-Arg-Thr-Gly-Arg-Arg-Asn-Ser-Ile) (*38*) (Upstate Biotechnology), protein kinase C (PKC) (Phe-Lys-Lys-Ser-Phe-Lys-Leu) (*39*) (GibcoBRL), calcium calmodulin dependent protein kinase II (CaM PK II) (Syntide 2; Pro-Leu-Ala-Arg-Thr-Leu-Ser-Val-Ala-Gly-Leu-Pro-Gly-Lys-Lys) (*40*) synthesized by University of Florida's ICBR Proteomics Core, casein kinase I (Arg-Arg-Lys-Asp-Leu-His-Asp-Asp-Glu-Glu-Asp-Glu-Ala-Met-Ser-Ile-Thr-Ala) (*41*) (CalBiochem) and casein kinase II (Arg-Arg-Ala-Asp-Asp-Ser-Asp-Asp-Asp-Asp-Asp) (*41*) (CalBiochem). The proteins assayed—α and β casein and phosvitin—are substrates for a variety of kinases. Full-length *Limulus* visual arrestin and the C-terminus of *Limulus* opsin (from H^{332} to A^{376}), phosphoproteins involved in the *Limulus* photoresponse, were expressed as described previously (*37*, *42*). The loop 2 region of LpMYO3 and mutants of this region that were tested as substrates for rLpMYO3 were prepared as described above.

Phospho-Amino Acid Identification and the Generation and Analysis of Two-Dimensional (2D) Tryptic Phosphopeptide Maps. Phosphorylated amino acids were identified using protocols describe by Boyle et al. (*43*). The tryptic digestion of proteins and the production and analysis of 2D tryptic phosphopeptide maps were performed as described by Sineschchekova et al. (*28*) with 0.2 μg of trypsin added at the start of trypsinization and again 3 h later.

Recovery, Purification, and Identification of Peptides from the 2D Maps. The most highly phosphorylated tryptic phosphopeptide released from rLpMYO3 was located on the TLC plate and recovered as described by Boyle et al. (*43*). The extracted peptide was purified over a gallium affinity column (Pierce Biotechnology) as described by the manufacturer with 87% recovery. The recovered peptide was then analyzed by matrix-assisted laser desorption/ionization (MALDI) quadrupole time-of-flight mass spectrometry (qTOFMS) (QSTAR XL, Applied Biosystems). Prior to MALDI-qTOFMS analysis, the tryptic peptide was bound to a custom packed oligo R3 reversed phase (Applied Biosystems) microcolumn, washed several times with 0.1% trifluoroacetic acid (TFA), and eluted onto a MALDI target with 1 μL of matrix solution. The matrix solution was prepared by dissolving 5 mg of α-cyano-4-hydroxycinnamic acid (Sigma-Aldrich) in 1 mL of 50% acetonitrile/0.1% TFA. Full scan

mass spectra were acquired for several minutes using a N_2 laser operated at 20 Hz. For collision induced dissociation experiments in which MALDI was the source of ion production, the collision energy was maintained at 95 eV using nitrogen as the collision gas.

Mass Spectrometric (MS) Analysis of Phosphorylation Sites in Full-Length rLpMYO3. Purified rLpMYO3 was phosphorylated with PKA as described above and gel purified. The Coomassie Blue-stained rLpMYO3 band was cut from the gel and subjected to in-gel digestion with trypsin according to a protocol used by the University of Florida's Interdisciplinary Center for Biotechnology Research (ICBR) Proteomics Core Facility (Gainesville, FL). Capillary reversed-phase (rp) HPLC separation of the rLpMYO3 tryptic digest was performed on a 15 cm × 75 μm i.d. PepMap C18 column (LC Packings) in combination with an Ultimate Capillary HPLC System (LC Packings) operated at a flow rate of 200 nL/min. A PepMap C18 capillary trap was used in combination with the Switchos isocratic solvent delivery pump in order to concentrate and desalt the sample prior to LC/MS/MS analysis. A gradient flow rate of 200 nL/min was obtained by splitting a flow of 180 μL/min provided by the gradient HPLC pump. Solvent A was 0.1% acetic acid in 95% water/5% acetonitrile, and solvent B was 0.1% acetic acid in 10% water/90% acetonitrile. Following isocratic solvent delivery for 5 min during the sample desalting step, a linear gradient was carried out for 60 min to 40% solvent B. Inline MS analysis was accomplished by a hybrid qTOFMS instrument (QSTAR) equipped with a nanoelectrospray source. The information-dependent acquisition (IDA) mode of operation was employed in which a survey scan from *m*/*z* 400 to 1500 was acquired followed by collision-induced dissociation of the three most intense ions. Survey and MS/MS spectra for each IDA cycle were accumulated for 1 and 3 s, respectively.

MS/MS spectra generated from the IDA analysis on the QSTAR instrument were searched against the NCBI non-redundant protein sequence database using the Mascot (Matrix Science, Boston, MA) search algorithm. Phosphorylation of serine and threonine was allowed as a variable modification in the database search. MS/MS spectra corresponding to phosphopeptides identified from the Mascot search were validated using the in silico MS/MS fragmentation program MS-Product available at ProteinProspector (http://prospector.ucsf.edu).

Characterization of Actin Binding and ATPase Activity. Binding of rLpMYO3 to F-actin was assayed by cosedimentation. Full-length rLpMYO3 was mixed with different concentrations of phalloidin-stabilized actin prepared from rabbit skeletal muscle (*44*) in the absence of ATP. Incubations were for 5 min at room temperature in buffer containing 20 mM MOPS pH 7.0, 5 mM $MgCl_2$, 0.05 mM EGTA, 1 mM NaN_3, 1 mM DTT and 0.1 M NaCl. Following centrifugation at 100,000 × *g* and 4 °C, pellets and supernatants were fractionated on 4−20% SDS polyacrylamide gels, and gels were stained with Coomassie Blue and analyzed by densitometry. Data points were fitted to a quadratic equation OriginLab 7.0 (Microcal Corp.). The actin-activated ATPase activity of LpMYO3 was assayed with an NADH-coupled assay (*45*) in the presence of 1 μM Δkinase LpMYO3, 1 mM ATP, and 40 μM actin. Inhibition of skeletal S1 (0.1 μM) actin-activated ATPase activity by Δkinase LpMYO3 was also assayed in an NADH-coupled assay (*45*) at various concentrations of Δkinase LpMYO3, 1 μM actin and 1 mM ATP. Skeletal S1 was prepared from rabbit skeletal muscle (*46*).

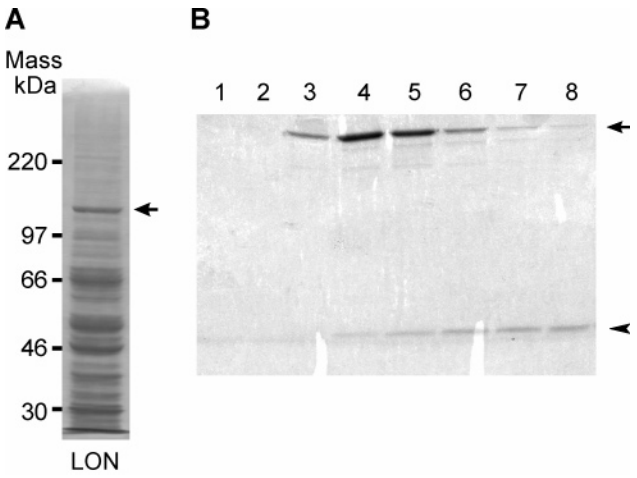

FIGURE 1: (A) Proteins in lateral optic nerve (LON) soluble fraction. A Coomassie Blue-stained 7.5% SDS gel is shown. The locations of the molecular mass standards are indicated on the left. The arrow points to the LpMYO3 band. LpMYO3 is a prominent protein in soluble fractions of LON. (B) Purification of full-length rLpMYO3 by FLAG-affinity chromatography. Full-length LpMYO3 was expressed together with *Drosophila* calmodulin in the baculovirus/sf9 system. A FLAG sequence added to the 3′ end of the LpMYO3 construct permitted purification by FLAG affinity chromatography. Shown is a Coomassie Blue-stained 15% SDS gel of proteins in aliquots of fractions eluted from the FLAG affinity column with FLAG peptide. The fraction numbers are shown at the top of the gel. Two major bands are seen, rLpMYO3 (arrow) and calmodulin (arrowhead). Calmodulin did not elute exactly with rLpMYO3.

RESULTS

The LpMYO3 used in this study came from several sources, endogenous protein from LON or ventral eyes and rLpMYO3 heterologously expressed in sf9 cells. A high concentration of LpMYO3 in extracts of *Limulus* eyes and optic nerves (Figure 1A) facilitated analyses of the endogenous protein. In SDS PAGE, LpMYO3 migrates as a prominent Coomassie Blue-stained band with an apparent molecular mass of 122 kDa. Previous 2D separations of LE and ventral photoreceptor proteins showed that this band contains a single protein (*20*).

Figure 1B shows a representative Coomassie Blue-stained SDS polyacrylamide gradient gel (4−20%) of full-length rLpMYO3 obtained during its purification from sf9 cells by FLAG affinity chromatography. Only two proteins were detected, full-length rLpMYO3 and the calmodulin with which it was coexpressed. Although LpMYO3 has one IQ domain, calmodulin typically did not copurify with rLpMYO3 suggesting that the affinity of rLpMYO3 for calmodulin is low.

PKA and Autophosphorylation of rLpMYO3. Like the endogenous protein (*3*, *20*), rLpMYO3 was phosphorylated by PKA (Figure 2A). It also underwent autophosphorylation (Figure 2B). Both PKA and autophosphorylation of rLpMYO3 occurred on serine residues (data not shown), and autophosphorylation was intermolecular (Figure 2C).

Identification of PKA Phosphorylation Sites. A concern was whether PKA phosphorylates recombinant and endog-

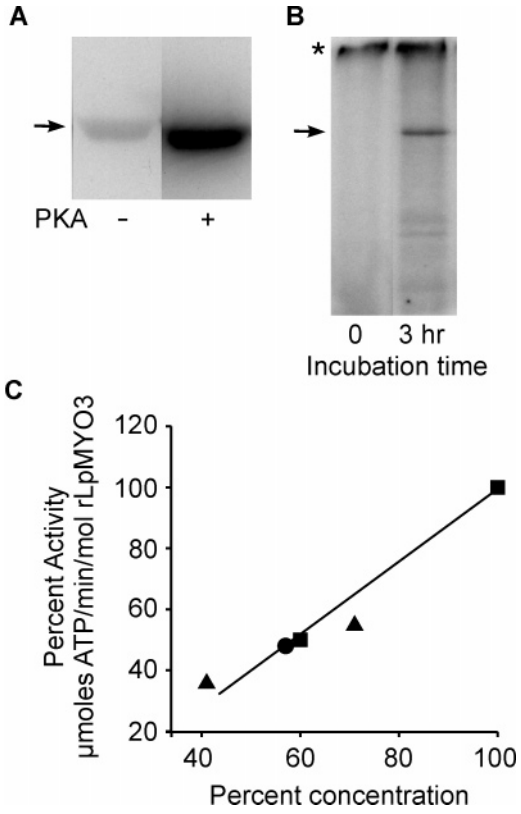

FIGURE 2: PKA phosphorylation and autophosphorylation of rLpMYO3. (A) Phosphorimage of 20 μg of full-length rLpMYO3 that had been incubated for 5 min with [γ^{32}P] ATP in the absence (−) or presence (+) of the catalytic subunit of PKA (8 units) then separated by SDS PAGE. The location of rLpMYO3 is indicated (arrow). (B) Phosphorimage of 2 μg of full-length rLpMYO3 separated by SDS PAGE after it had been incubated for zero time and 3 h with [γ^{32}P] ATP under autophosphorylating conditions. The location of rLpMYO3 is indicated (arrow). The asterisk (*) indicates the top of the gel where some free radiolabeled ATP typically sticks. (C) Graph showing that autophosphorylation of rLpMYO3 is intermolecular. The rate of rLpMYO3 autophosphorylation was measured as μmol of ATP incorporated per min per mol of rLpMYO3 incubated. At least two different concentrations of three different preparations of rLpMYO3 (■, ●, ▲) were assayed. The activity of the highest concentration (approximately 0.4 μM) of each preparation assayed was set at 100%, and each dilution is shown on the *X* axis as a percent of the maximum concentration. The activity of each dilution is expressed on the *Y* axis as a percent of the maximum activity.

enous LpMYO3 on the same sites. To test this we compared 2D tryptic phosphopeptide maps of recombinant and endogenous LpMYO3 following PKA phosphorylation. 2D tryptic phosphopeptide maps obtained from rLpMYO3 phosphorylated by PKA and from endogenous LpMYO3 phosphorylated by PKA in LON homogenates consistently showed a single heavily labeled phosphopeptide and a number of less heavily labeled phosphopeptides. The phosphopeptides from both protein sources comigrated in mixing experiments (Figure 3A). The tryptic phosphopeptides obtained from endogenous LpMYO3 phosphorylated by activation of the cAMP cascade in intact cells also produced a similar 2D map (Figure 3B). These findings provide strong evidence that rLpMYO3 and endogenous LpMYO3, both in homogenates and in intact cells, are phosphorylated by PKA on the same tryptic peptides.

Previous studies showed that at least some PKA phosphorylation sites in endogenous LpMYO3 are located in the myosin domain (*3*). To test whether the kinase domain might also contain PKA phosphorylation sites we compared 2D maps of tryptic phosphopeptides from PKA-phosphorylated full-length and Δkinase rLpMYO3. These maps, which were like those in Figure 3, appeared identical to one another, and all phosphopeptides from both proteins comigrated in mixing experiments (data not shown). This result indicates that all PKA phosphorylation sites in LpMYO3 are within the myosin or tail domains. The myosin domain of LpMYO3 contains three putative PKA phosphorylation sites (*3*) (Figure 4A). All are in or near loop 2, an important actin binding region of other myosins (*47*). The short tail domain of LpMYO3 contains no potential PKA phosphorylation sites (*3*).

The most heavily labeled phosphopeptide observed on 2D maps of PKA phosphorylated endogenous and rLpMYO3 was collected from six 2D phosphopeptide maps of rLpMYO3 and processed for analysis by mass spectrometry. The sequence of the peptide obtained by fragment ion analysis matched exactly a peptide within loop 2, and S^{846} was identified as the phosphorylated residue (Figures 4A and 4B). Thus S^{846} is a major site for PKA phosphorylation in both the recombinant and endogenous proteins.

The presence of two additional predicted PKA phosphorylation sites in the myosin domain of LpMYO3 and multiple phosphopeptides in the 2D maps of PKA phosphorylated rLpMYO3 (Figure 3) might mean that multiple sites are phosphorylated by PKA. However, the maximum PKA-stimulated molar incorporation of [γ ^{32}P] ATP into rLpMYO3 was less then one. A likely explanation is that rLpMYO3 becomes partially phosphorylated in the sf9 cells. Indeed, we found that incubating sf9 cells with ^{32}P-labeled inorganic phosphate during rLpMYO3 expression produced ^{32}P-labeled rLpMYO3 (Figure 5).

As an alternative approach to determining whether PKA can phosphorylate the other two putative PKA sites, we expressed the region of LpMYO3 containing all three potential sites (from N^{781} to D^{940}, see Figure 4A) in *E. coli* to produce polypeptides that are not post-translationally modified. Four variants of this loop 2 region polypeptide were expressed and tested as substrates for PKA (Figure 6). One contained all three putative PKA phosphorylation sites (wild-type); three each contained only one site, and another contained none. In each case the serine residues eliminated were replaced with alanine residues. Our results show that S^{846} was phosphorylated at a rate nearly the same as that of the wild-type. S^{796} was also phosphorylated but at a much slower rate (10% of wild-type), and no phosphate was incorporated into the construct containing S^{926} only or into the construct lacking all three predicted PKA phosphorylation sites. The last observation confirms that no additional PKA phosphorylation sites are present in this region.

Surprisingly MS analysis of PKA-phosphorylated full-length rLpMYO3 showed that, in addition to the predicted pS^{846} and pS^{796}, S^{841} was phosphorylated (Figure 7). S^{841} is a predicted PKC site located within loop 2. This site must become phosphorylated in sf9 cells by a kinase other than PKA.

Characterization of LpMYO3 Kinase Activity and Identification of an Autophosphorylation Site. As is shown in Figure 2, rLpMYO3 undergoes intermolecular autophosphorylation. To begin to characterize LpMYO3 kinase activity,

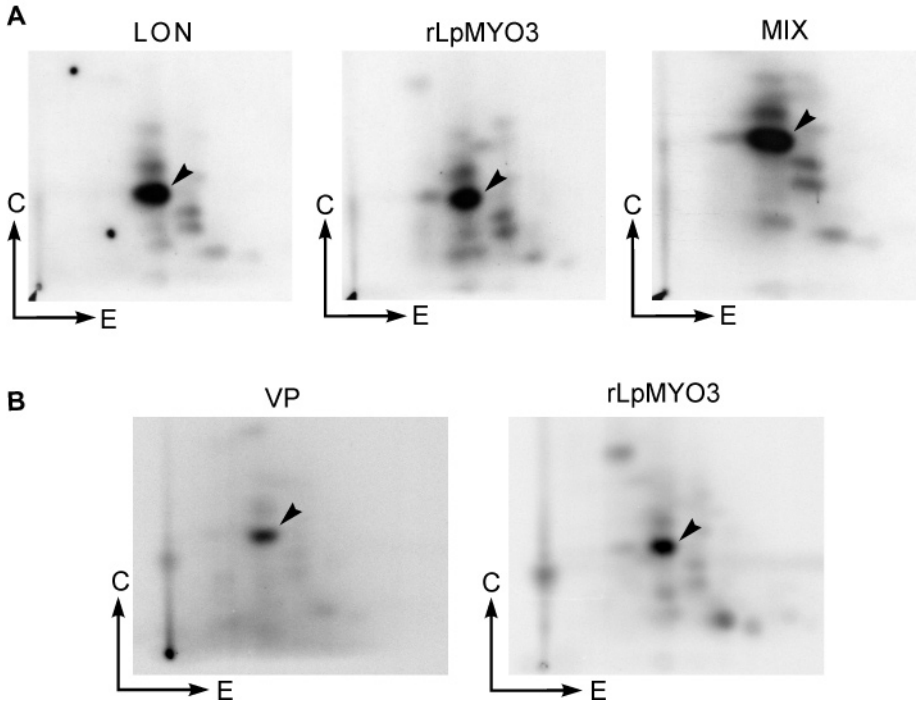

FIGURE 3: Two-dimensional (2D) maps of phosphopeptides released from endogenous and full-length rLpMYO3. (A) Phosphorimages of 2D tryptic phosphopeptide maps generated from gel purified rLpMYO3 and endogenous LpMYO3 from lateral optic nerve (LON) homogenates. Both proteins were phosphorylated with PKA in the presence of [γ^{32}P]ATP. Tryptic phosphopeptides released from recombinant and endogenous LpMYO3, and containing roughly the same amounts of radioactivity, were mixed and run together (MIX). (B) Phosphorimages of 2D tryptic phosphopeptide maps generated from gel purified endogenous LpMYO3 from intact ventral photoreceptors (VP) that had been phosphorylated in response to activation of adenylyl cyclase by forskolin and rLpMYO3 that had been phosphorylated by PKA. All maps show a similar distribution of phosphopeptides. In particular, each contains one heavily labeled phosphopeptide (arrowhead) in the same position relative to the other phosphopeptides. E, direction of electrophoresis; C, direction of ascending chromatography.

we tested the ability of full-length rLpMYO3 to phosphorylate peptides that are substrates for other kinases. rLpMYO3 phosphorylation of the preferred peptide substrate for PKA was linear with time up to 2 h (not shown) and substrate concentration up to 5 μM substrate (Figure 8A). But LpMYO3 did not phosphorylate preferred substrates for PKC, CaM PK II, or casein kinase I and II (see Experimental Procedures for peptide sequences and references). rLpMYO3 phosphorylation of the PKA peptide substrate was inhibited by the pseudosubstrate peptide inhibitor of PKA (PKI) (*38*) with half-maximal inhibition at about 0.1 μM and by H89 (*48*) (BioMol) and KT5720 (*49*) (Figure 8B,C). Half-maximal inhibition was achieved with about 0.2 μM of the latter compounds which are competitive inhibitors of ATP binding to PKA.

LpMYO3 autophosphorylation was also inhibited by H89 and PKI (Figure 8D). The percent of maximum autophosphorylation observed in the presence of 1 μM H89 and 0.2 μM PKI was 24.5 $\pm$ 3.5 and 10.5 $\pm$ 0.5, respectively (mean $\pm$ the standard error of the mean for 4 assays). Autophosphorylation was not inhibited by 100 μM of autoinhibitory peptides of PKC (PKC 19−36) (*50*) or CaM PK II (CaM PKII 273−302) (*51*) or by 0.2 μM of calphostin C (BioMol) or RO-31-8220 (BioMol), competitive inhibitors of ATP binding to PKC (*52*), and several other kinases (*53*). Thus, LpMYO3 and PKA have overlapping substrate specificities and share some pharmacological properties.

rLpMYO3 also phosphorylated protein substrates (Figure 9). β casein and phosvitin contain putative PKA phosphorylation sites while α casein does not (ScanProsite: http://www.expasy.ch/cgi-bin/scanprosite); therefore the substrate

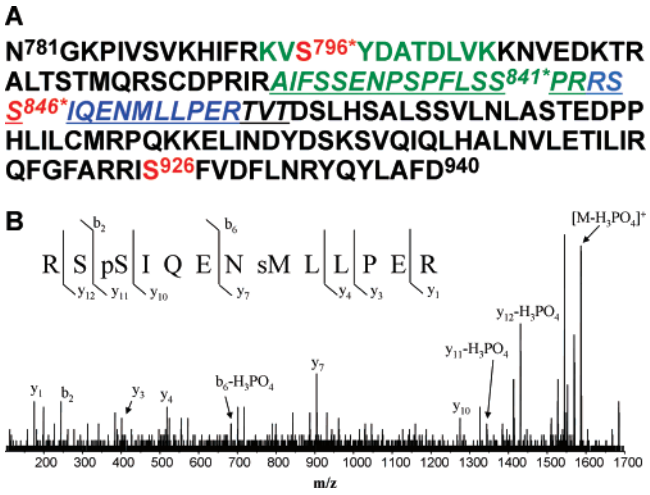

FIGURE 4: (A) Amino acid sequence of LpMYO3 in the region of the myosin domain containing the three predicted PKA phosphorylation sites (in red): S^{796}, S^{846}, S^{926}. The sequence of loop 2 is in italics and underlined. In blue is the sequence of the most heavily labeled phosphopeptide recovered from maps of PKA-phosphorylated rLpMYO3 (Figures 3 and 4B). In green are additional phosphorylated peptides detected by mass spectrometry from PKA-phosphorylated full-length rLpMYO3 (Figure 7). The full sequence shown, called the loop 2 region of LpMYO3, was also expressed in *E. coli* and tested as a substrate for PKA phosphorylation (Figure 6) and phosphorylation by rLpMYO3 (see text). (B) MS/MS analysis of the major PKA-phosphorylated tryptic peptide collected from 2D maps. The most heavily labeled phosphopeptide observed on the 2D maps shown in Figure 3 was collected from 6 separate plates, purified, and analyzed by MALDI quadrupole time-of-flight mass spectrometry. Peaks are labeled according to Beimann (*54*) nomenclature; pS, phosphoserine; sM, doubly oxidized methionine (sulfone).

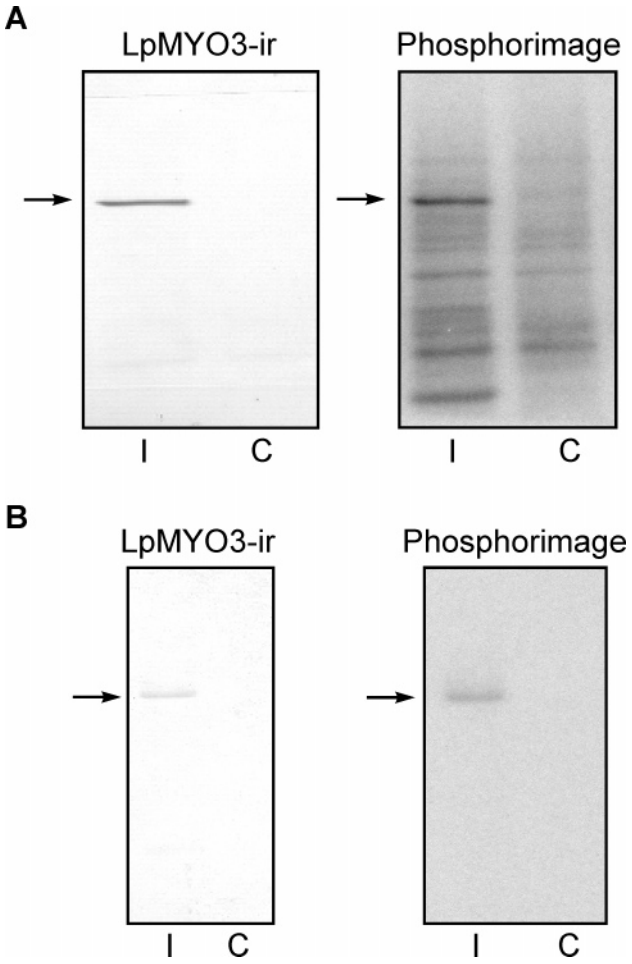

FIGURE 5: rLpMYO3 phosphorylation in sf9 cells. (A) Blots of homogenates of uninfected control sf9 cells (C) and sf9 cells that had been infected (I) with baculovirus for the expression of full-length rLpMYO3 and calmodulin were immunostained for LpMYO3 immunoreactivity (arrow) and then exposed to a phosphorimaging screen to detect incorporated ^{32}P. Infected and control cells had been incubated with $^{32}PO_4$ overnight at room temperature prior to homogenization; an aliquot of each homogenate was subjected to SDS PAGE and Western blotting. (B) Blots of affinity purified rLpMYO3 from infected (I) and control (C) cells that had been incubated with $^{32}PO_4$ and processed as described in A. The location of rLpMYO3 is indicated (arrow).

specificity of LpMYO3 may be broader than that of PKA. Interestingly, while α casein was an excellent substrate for rLpMYO3, dephosphorylated α casein was not. This could mean that the ability of LpMYO3 to phosphorylate a site is enhanced by the presence of phosphate groups at nearby sites.

We then asked whether LpMYO3 could phosphorylate *Limulus* visual arrestin or *Limulus* opsin, two phosphoproteins involved in the photoresponse. LpMYO3 failed to phosphorylate visual arrestin, but it did phosphorylate the C-terminus of *Limulus* opsin (Figure 9B) on serine residues (not shown).

We next sought to identify autophosphorylation sites in LpMYO3. Figure 10 compares 2D tryptic phosphopeptide maps from autophosphorylated and PKA-phosphorylated rLpMYO3. The phosphopeptide maps appeared identical to one another, and the phosphopeptides comigrated in mixing experiments. Of particular interest is the heavily labeled phosphopeptide released from the autophosphorylated protein that comigrated with the major PKA-phosphorylated peptide

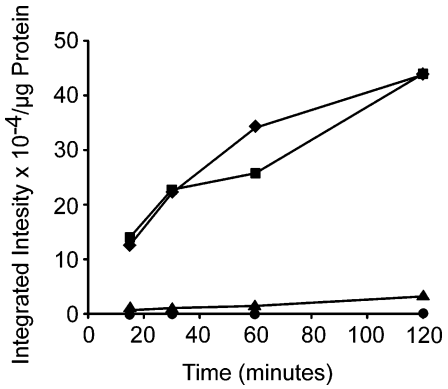

FIGURE 6: PKA phosphorylation of wild-type and mutant sequences of the loop 2 region of LpMYO3 expressed in *E. coli*. Wild-type and mutant sequences of the loop 2 region of LpMYO3 (Figure 4A) (10−12 μg each) were incubated for the times indicted under phosphorylating conditions with [γ^{32}P] ATP and 8 units of the catalytic subunit of PKA. Radioactivity associated with the loop 2 region polypeptide was detected with a phosphorimager and quantified with ImageQuant from dried, Coomassie Blue-stained SDS gels. The integrated intensity of the radioactive signal was normalized to the exact amount of substrate incubated as determined from scans of the protein stain also analyzed with ImageQuant. Each point is the result of a single assay. Similar results were obtained in three separate experiments. (◆) Wild-type sequence containing all three predicted PKA phosphorylation sites. Each mutant sequence contained only one predicted PKA phosphorylation site. (■) S^{846}, (▲) S^{796}, (●) S^{926}.

we identified above as containing pS^{846} (Figures 3 and 4B). We conclude that autophosphorylation, like PKA phosphorylation, targets S^{846} within loop 2 of the myosin domain. This conclusion is supported by the results of assays of the rate at which rLpMYO3 phosphorylated wild-type and mutant loop 2 region polypeptides purified from *E. coli*. The mutant containing S^{846} was clearly the preferred substrate for rLpMYO3, and the rates of phosphorylation of the mutants containing S^{796} or S^{926} were 70% and 30% of that measured for the S^{846} mutant, respectively.

Assays of LpMYO3 Actin Binding and ATPase Activities. The ability of full-length rLpMYO3 to bind actin was assayed by actin cosedimentation. rLpMYO3 cosedimented with actin in the absence of ATP. Figures 11A and B show the quantitative titration curves resulting from densitometry on the cosedimentation gels. A quadratic equation was fitted to the data points. Note that rLpMYO3 could not be saturated with actin (maximum fractional binding is 0.7 μM). A subsequent pulldown assay performed with the first supernatant again showed that only approximately 70% of the myosin bound to actin. This indicates that the failure of a subpopulation of rLpMYO3 to bind to actin cannot be attributed to denaturation of the myosin and probably represents an equilibrium between a conformation capable of binding to actin and a conformation that cannot bind. The K_d value determined (∼0.1 μM) has to taken as an approximation since we cannot work at the lower actin and myosin concentrations (1−20 nM) required to make an accurate determination using actin sedimentation assays. To test whether the binding of rLpMYO3 to actin was sensitive to ATP, we examined the ability of its myosin domain to inhibit the actin-activated MgATPase activity of skeletal muscle S1. As rLpMYO3 binds to actin, it will reduce the effective concentration of actin available to interact with skeletal muscle myosin in a concentration dependent manner.

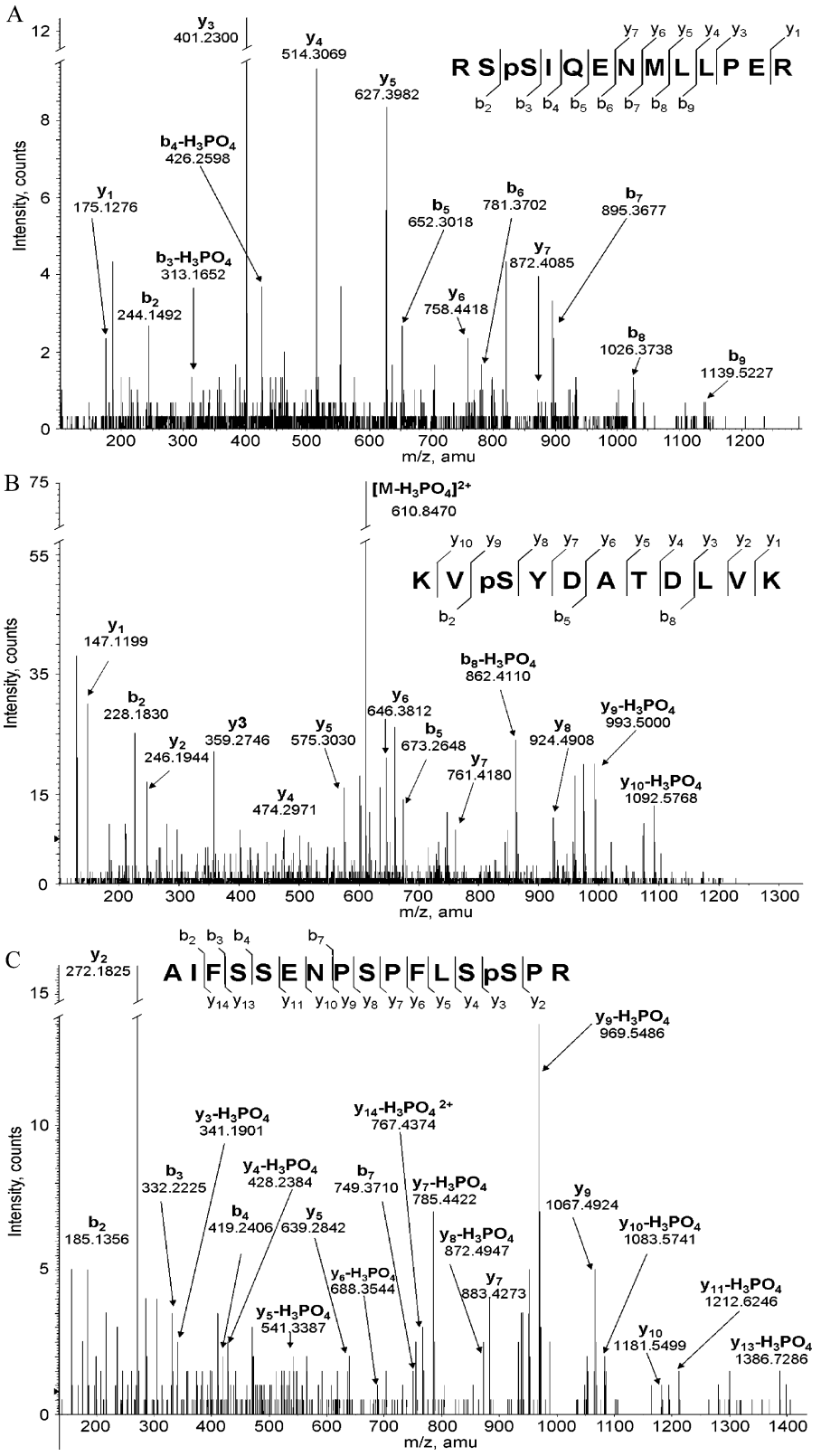

FIGURE 7: MS/MS analysis of phosphopeptides obtained from a tryptic digest of full-length rLpMYO3 phosphorylated with PKA. The tryptic digest was analyzed by LC/MS/MS as described in Experimental Procedures using a hybrid quadrupole time-of-flight instrument (QSTAR) equipped with a nanoelectrospray source. The tryptic peptide sequence and sites of serine phosphorylation (pS) were identified after searching the MS/MS spectra against the NCBI nr database using the Mascot search algorithm. Peaks are labeled according to Beimann (*54*) nomenclature using Mascot standard output. (A) RSpSIQENMLLPER, (B) KVpSYDATDLVK, (C) AIFSSENPSPFLSpSPR.

From this assay, which was done in the presence of 1 mM ATP, we determined a K_i for rLpMYO3 of 0.09 μM (Figure 11C), which is similar to the value of 0.1 μM determined in the direct binding assay performed in the absence of ATP. The finding that the affinity of LpMYO3 for actin was not reduced in the presence of ATP suggested that LpMYO3 lacks ATPase activity. Therefore, the actin-activated ATPase activity of Δkinase rLpMYO3 was tested directly with an

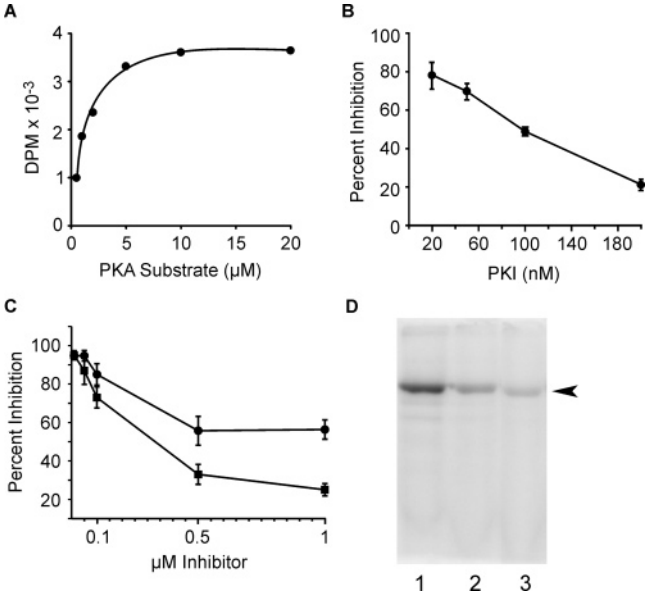

FIGURE 8: rLpMYO3 kinase activity. Unless otherwise specified, the concentrations of rLpMYO3 and PKA peptide substrate in each assay were 0.4 μM and 5 μM, respectively; incubations were for 1 h. (A) Concentration dependence of the phosphorylation of the PKA peptide substrate by rLpMYO3. The concentration of PKA peptide substrate incubated is plotted against the DPM of ^{32}P incorporated into the peptide assayed by the phosphocellulose binding assay. (B) rLpMYO3 phosphorylation of the peptide substrate was assayed as described in A with increasing concentrations of PKI. The concentration of PKI in the assay is plotted against the percent of phosphorylation observed in the absence of inhibitor (100%). (C) rLpMYO3 phosphorylation of the PKA peptide substrate assayed as described in A with increasing concentrations of H89 (■) or KT5720 (●). The concentration of inhibitor is plotted against the percent of phosphorylation observed in the absence of inhibitor. In B and C, data points are the means ± the standard errors of the means for at least 3 determinations. (D) Phosphorimages of rLpMYO3 autophosphorylation in the absence (lane 1) and presence of 1 μM H89 (lane 2) or 0.2 μM PKI (lane 3). Incubations were for 3 h.

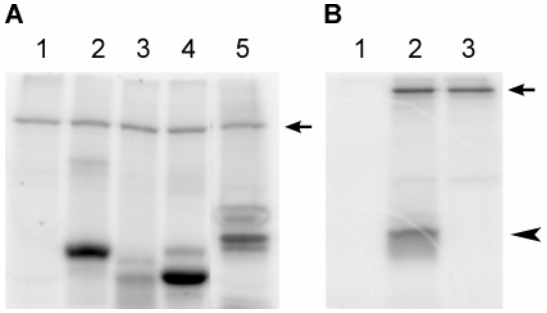

FIGURE 9: rLpMYO3 phosphorylation of protein substrates. (A) Phosphorimages showing the results of 3 h incubations of rLpMYO3 (0.4 μM) with [γ^{32}P] ATP alone (lane 1), or with 10 μM each of α casein (lane 2), dephosphorylated α casein (lane 3), β casein (lane 4), and phosvitin (lane 5). (B) Phosphorimage showing the results of a 3 h incubation of rLpMYO3 (0.4 μM) with [γ^{32}P] ATP alone (lane 3) or with the C-terminus of *Limulus* opsin (approximately 50 μM) (lane 2). The opsin C-terminus was also incubated alone (lane 1). Autophosphorylated rLpMYO3 is indicated with an arrow. In B, the location of the opsin C-terminus is indicated with an arrowhead.

NADH-coupled assay. Figure 11D shows that the slopes of the linear fits of the rates of ATP hydrolysis measured in the absence and presence of Δkinase rLpMYO3 were identical within the error range implying that rLpMYO3 does not hydrolyze ATP at a significant rate. We also assayed the ATPase activity of other rLpMYO3 constructs (full-length and tailless) in the presence or in the absence of actin (the so-called basal ATPase activity). We could not detect hydrolytic activity in any of the rLpMYO3 preparations in any conditions.

DISCUSSION

In this study we show that LpMYO3 is phosphorylated by PKA and by autophosphorylation within and near loop 2 of its myosin domain, a major actin binding region (*47*). A second phosphorylation site we identified within loop 2 is a predicted substrate for PKC. In addition to phosphorylating itself, we found that LpMYO3 can phosphorylate other substrates, thus it can serve as a signaling molecule with broad substrate specificity. We found that LpMYO3 can bind to actin. However, since its affinity for actin is not detectably changed by ATP, and it apparently lacks ATPase activity, LpMYO3 is probably not a motor.

Identification of Phosphorylation Sites. Much evidence points to S^{846} within loop 2 as a major target for phosphorylation by both PKA and autophosphorylation. The tryptic phosphopeptide containing S^{846} was identified in a number of different experiments as a major target for PKA phosphorylation of recombinant and endogenous LpMYO3 and autophosphorylation of rLpMYO3 (Figure 3 and Figure 10). Two possible phosphorylation sites are located within this peptide, S^{845} and S^{846}, however multiple MS analyses detected only pS^{846}, the predicted PKA phosphorylation site. S^{846} was also the preferred substrate for PKA and autophosphorylation in phosphorylation assays which utilized as substrate the loop 2 region polypeptides expressed in *E. coli* (Figure 6), and in this same series of experiments, no phosphorylation was detected using the mutant that lacked all PKA phosphorylation sites but retained S^{841} and S^{845}. Thus we have no evidence for the phosphorylation of S^{841} or S^{845} by either PKA or autophosphorylation.

MS analyses of PKA-phosphorylated rLpMYO3 identified pS^{796}, the second best substrate for PKA phosphorylation and autophosphorylation in the loop 2 region polypeptides. Thus, S^{796} is also a likely site for both PKA mediated phosphorylation and autophosphorylation. MS analyses failed to detect pS^{926} in full-length rLpMYO3 expressed in sf9 cells, but this site was autophosphorylated at a low rate when the loop 2 polypeptide was used as a substrate. Thus it remains unclear whether this site is an important target for phosphorylation in the full-length protein.

MS analyses produced the surprising finding that S^{841}, a predicted PKC site located within loop 2, is phosphorylated in rLpMYO3. This is not an artifact of the heterologously expressed protein because MS analyses of endogenous LpMYO3 also consistently identifies pS^{841} (Cardasis, Stevens, and Battelle, unpublished). The kinase responsible for the phosphorylation of this site is not yet known. S^{841} is not phosphorylated by PKA (Figure 6) or autophosphorylation; however it may be a substrate for PKC. In this regard, it is interesting to note that the phosphorylation of endogenous LpMYO3 in intact cells is enhanced by light (*55*) as well as by clock input, and in rhabdomeral photoreceptors, light is thought to activate PKC (*56*, *57*). Studies are in progress to test whether S^{841} is a light-regulated PKC site.

The phosphorylation of sites within loop 2 is interesting because in other myosins the net charge of loop 2 is a major

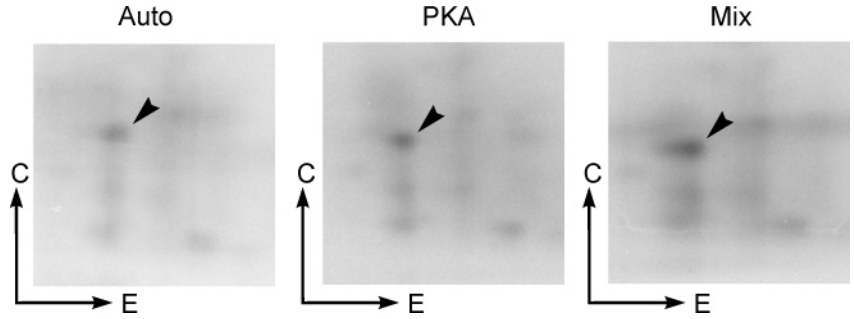

FIGURE 10: Phosphorimages of 2D maps of tryptic phosphopeptides from autophosphorylated and PKA-phosphorylated full-length rLpMYO3. Full-length rLpMYO3 that had been autophosphorylated (Auto) or phosphorylated by PKA (PKA) were gel purified and digested with trypsin. The tryptic peptides were separated as described in Experimental Procedures, and phosphopeptides were visualized with a phosphorimager. The third phosphorimage (Mix) shows the map obtained after mixing peptides obtained from autophosphorylated and PKA-phosphorylated rLpMYO3. Equal counts from the two samples were mixed. The arrowhead points to the major PKA-phosphorylated tryptic peptide.

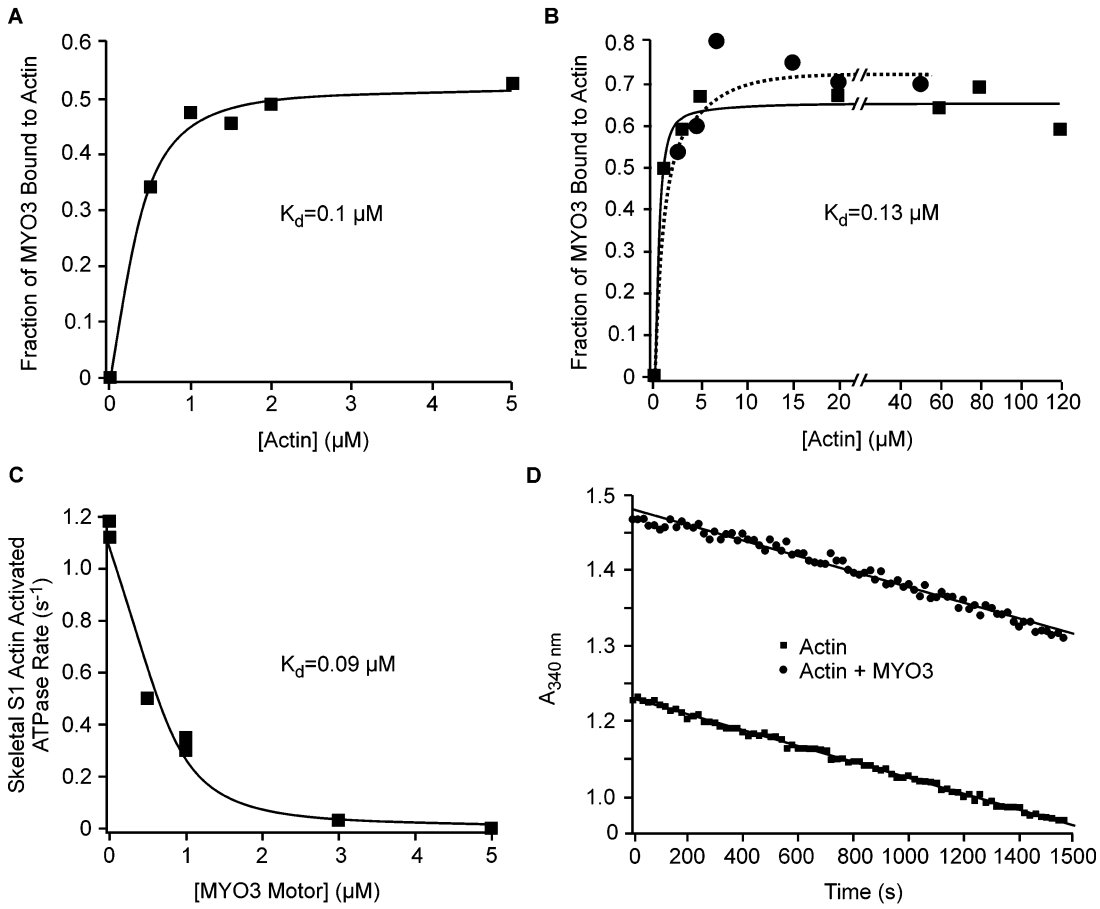

FIGURE 11: rLpMYO3 actin binding and ATPase activities. (A) 0.5 μM full-length rLpMYO3 was mixed with various concentrations of phalloidin-stabilized actin and centrifuged at 100,000 $\times$ *g*. Pellets and supernatants were run on 4−20% SDS PAGE gels, stained, and evaluated by densitometry. Data points were fitted to a quadratic equation. (B) Two experiments similar to A except 1 μM (■) and 0.86 μM (●) rLpMYO3 and higher actin concentrations were used. The gel from which the data in the solid circles (●) were obtained is shown in the Supporting Information. (C) The steady-state ATPase activity of 0.1 μM skeletal S1 with 1 μM actin was measured by a NADH-coupled assay at various rLpMYO3 motor domain concentrations. The decrease in actin activation of skeletal S1 ATPase is due to rLpMYO3 binding to actin. A quadratic equation fits the data with a K_d similar to the ones obtained in the direct actin binding experiments. (D) An NADH-coupled assay was used to investigate the ATPase activity of the rLpMYO3 motor domain. The curves were obtained at 1 mM ATP and 40 μM actin concentration. The slopes of the linear fits are identical within the error range implying that rLpMYO3 does not hydrolyze ATP.

factor influencing actomyosin interactions. A higher number of net positive charges in loop 2 correlates with increased actin binding affinity (*58*, *59*). The net charge of amino acids in loop 2 of LpMYO3 is zero; phosphorylation will drive the net charge into the negative range. This leads us to predict that the affinity of LpMYO3 for actin will be low compared to other myosins even when not phosphorylated in loop 2, and that loop 2 phosphorylation will reduce this affinity still further. In addition, the *Dictyostelium* myosin II equivalent residue of S^{796} in LpMYO3 is on the actin binding surface of the motor; therefore phosphorylation of this residue may also influence actomyosin interactions.

Assays of LpMYO3's Myosin-like Properties. The affinity of rLpMYO3 for actin measured in the absence of ATP

(Figure 11A,B) is low compared to that of other myosins (*60*). However, the significance of the absolute affinity measured is not clear since we have shown that rLpMYO3 purified from sf9 cells is at least partially phosphorylated (Figure 5). Our consistent observation that rLpMYO3 cannot be saturated with actin suggests that our preparations contain a mixture of molecules in a state competent to bind to actin and a state that does not bind to actin, and that there is a slow equilibrium among the subpopulations. Similar findings have been described for myosin 9B (*61*). Attempts to test actin binding affinities of rLpMYO3 following phosphorylation and dephosphorylation were unsuccessful because the protein was unstable following these treatments. Ongoing experiments are comparing the actin binding affinities of LpMYO3 mutants in which the phosphorylation sites are either eliminated by conversion to neutral amino acids or mimicked by conversion to acidic amino acids.

More significant than the absolute actin binding affinities measured are our findings that the affinity of LpMYO3 for actin is the same in the presence and absence of ATP and that the LpMYO3 myosin domain lacks ATPase activity (Figure 11). The lack of ATPase activity is consistent with the primary sequence of LpMYO3. LpMYO3 lacks amino acids which in other myosins are essential for the catalysis of ATP hydrolysis. In the *Dictyostelium* myosin II motor domain, formation of the $E^{459}-R^{238}$ salt bridge enables the amide-NH of G^{457} to coordinate the γ phosphate of ATP leading to the hydrolysis-competent state. Mutation of either one of the salt bridge forming amino acids results in a dramatic loss of ATPase activity and in a slower rate of binding of fluorescent nucleotide analogues (*26*). Similar data were found in smooth muscle myosin where mutation of the arginine resulted in a myosin that could bind, but not hydrolyze ATP and which dissociated only poorly from actin in the presence of ATP (*27*). LpMYO3 has an H instead of an R at the equivalent position (*3*), which is consistent with its lack of enzymatic activity and the lack of effect of ATP on its binding to actin. These observations lead us to propose that LpMYO3 is an actin binding protein but not a motor. This hypothesis will be tested further using rLpMYO3 mutants in which the phosphorylation of specific sites is either blocked or mimicked with appropriate amino acid substitutions.

Comparisons between LpMYO3 and Other Class III Myosins. Most information about the biochemical properties of other class III myosins comes from studies of *Drosophila* NINAC (*62*) and human myosin 3A (hMYO3A) (*63*−*65*). NINAC, hMYO3A, and LpMYO3 are all protein kinases that autophosphorylate and phosphorylate other substrates; therefore all are signaling molecules. All three autophosphorylate within their myosin domains, indicating that they may modulate their own myosin-like properties. In fact, recent studies of hMYO3 suggest that the presence of the kinase domain, or phosphorylation of the myosin domain by the kinase domain, reduces the affinity of the myosin for actin (*64*, *65*). These observations are consistent with our predictions for LpMYO3. However, while LpMYO3 autophosphorylation is clearly intermolecular, autophosphorylation of hMYO3A is intramolecular (*63*). The mechanism of NINAC autophosphorylation is not yet known. The exact autophosphorylation sites in the NINAC and human MYO3A myosin domains are not yet known; however human MYO3A autophosphorylates within a C-terminal region of its myosin domain that includes a portion of loop 2 (*63*). Autophosphorylation within or near loop 2 may be a feature shared at least by LpMYO3 and hMYO3A.

All three class III myosins can phosphorylate other substrates, although relevant endogenous substrates have not been identified. Our studies identify LpMYO3 as a potential opsin kinase (Figure 8); however much additional work is needed to test whether opsin is a substrate for LpMYO3 in intact cells.

A salient feature of LpMYO3 that has not yet been identified in the other class III myosins is the PKA phosphorylation of its myosin domain within and near loop 2. No second messenger mediated phosphorylation has been reported within the myosin head domain of either NINAC or hMYO3A; however PKC phosphorylation of the NINAC tail domain has been described (*11*).

The ATP-independent actin binding observed with LpMYO3 is also distinctly different from human and fish MYO3A and NINAC, all of which show ATP-dependent actin binding (*7*, *63*−*65*). hMYO3A is also clearly a motor (*63*−*65*) whereas our evidence suggests that LpMYO3 is not. Motor activity for NINAC also has not yet been demonstrated. The salt bridge critical for ATP hydrolysis is conserved in NINAC (*2*); however lack of conservation in the ATP binding region of its motor domain leads to the speculation that NINAC is also not a motor.

Implications of LpMYO3 Phosphorylation for Limulus Photoreceptor Function. Studies of *Drosophila* suggest that MYO3 binds to and stabilizes the actin within the axial core of rhabdomeral microvilli. In *Drosophila* photoreceptors, NINAC typically decorates the actin in the rhabdomeral microvilli, and in *Drosophila* lacking NINAC, this actin is fragmented or missing even before eclosion (*10*, *66*). The PKA phosphorylation of sites within and near loop 2 of LpMYO3, which may modulate its affinity for actin, points to a role for LpMYO3 phosphorylation in regulating those circadian processes involving changes in the stability of the microvillar actin core. One such process is transient shedding of the photosensitive rhabdom (*23*, *24*, *67*).

Transient rhabdom shedding is characterized by the rapid, light-triggered breakdown and rebuilding of the actin-rich rhabdomeral microvilli. It results in the internalization or "shedding" of opsin-containing rhabdomeral membrane (*23*, *67*) and may rapidly convert the photoreceptor from a high to a low sensitivity state. Although transient rhabdom shedding is a light-triggered process, it must be "primed" by at least 3 h of prior clock input (*24*), elevated cAMP, and the activation of PKA (*68*).

We hypothesize that the "priming" of transient rhabdom shedding involves, in part, enhanced phoshorylation of S^{846}, and perhaps S^{796}, by PKA. LpMYO3 phosphorylation could reduce its affinity for actin and lead to reduced stability of the rhabdomeral actin core. A light-stimulated phosphorylation of the second site within loop 2, the predicted PKC site S^{841}, might be expected to further reduce the affinity of LpMYO3 for actin and thereby contribute to the light trigger for the breakdown of the actin microvilli. In fact, PKC localizes to the rhabdom in *Limulus* (*69*, *70*) and its activation triggers rhabdom breakdown in *Limulus* eyes that had been "primed" by clock input (*69*). Activation of PKC also leads

to the breakdown of rhabdomeral microvilli in several other arthropods (*71*−*73*).

We were surprised that LpMYO3 autophosphorylation targeted the same sites phosphorylated by PKA. However, since autophosphorylation is intermolecular, it may serve as a feedback mechanism regulating the concentration of LpMYO3 at the rhabdom during the day. Such a mechanism might be particularly important in *Limulus* photoreceptors in which the concentration of LpMYO3 is high.

Phosphorylation-regulated changes in the affinity of LpMYO3 for actin that modulate the concentration of LpMYO3 at the rhabdom could also lead to changes in the phosphorylation of other LpMYO3 substrates that participate in the photoresponse. This, in turn, could change the photoresponse. Consistent with this idea is the observation that *Drosophila* photoreceptors expressing NINACs that lack the kinase domain exhibit an abnormal photoresponse (*74*). Endogenous substrates for class III myoins are not yet known, but as we have shown (Figure 8), the C-terminus of *Limulus* opsin is a potential target.

SUMMARY

Our studies have revealed that the actin binding interface of LpMYO3 is a major target for phosphorylation by PKA, by LpMYO3 itself, and possibly by PKC. To the best of our knowledge this is the first report of any myosin becoming phosphorylated in this region. These phosphorylations may be a mechanism for regulating actomyosin interactions and particularly important for a myosin for which actin binding is not regulated by ATP. Our studies also show that LpMYO3 is a kinase and therefore a signaling molecule, and it may be an opsin kinase. Experiments in progress are designed to quantify changes in phosphorylation at individual sites *in vivo* in response to natural stimuli, something that is possible because of the high concentration of LpMYO3 in *Limulus* photoreceptors, and to determine the functional consequences of these phosphorylations on actin binding and other myosin-like properties. Endogenous substrates for the kinase domain of LpMYO3 are also being sought. Detailed characterizations of other class III myosins will be required to determine the extent to which their properties are similar to those of LpMYO3 including the phosphorylaton of the loop 2 region.

ACKNOWLEDGMENT

We thank Lynn Milstead for preparing figures.

SUPPORTING INFORMATION AVAILABLE

A Coomassie Blue stained gel from which data in Figure 11B were obtained. This material is available free of charge via the Internet at http://pubs.acs.org.

REFERENCES

1. Bähler, M. (2000) Are class III and class IX myosins motorized signaling molecules?, *Biochim. Biophys. Acta 1496*, 52−59.
2. Montell, C., and Rubin, G. M. (1988) The *Drosophila* ninaC locus encodes two photoreceptor cell specific proteins with domains homologous to protein kinases and the myosin heavy chain head, *Cell 52*, 757−772.
3. Battelle, B.-A., Andrews, A. W., Calman, B. G., Sellers, J. R., Greenberg, R. M., and Smith, W. C. (1998) A myosin III from *Limulus* eyes is a clock-regulated phosphoprotein, *J. Neurosci. 18*, 4548−4559.
4. De Velasco, B., Martinez, J. M., Ochoa, G. H., Miller, M. A., Clark, Y. M., Matsumoto, B., and Robles, J. L. (1999) Identification and immunolocalization of actin cytoskeletal components in light- and dark-adapted octopus retinas, *Exp. Eye Res. 68*, 725−737.
5. Dosé, A. C., and Burnside, B. (2000) Cloning and chromosomal localization of a human class III myosin, *Genomics 67*, 333−342.
6. Dosé, A. C., and Burnside, B. (2002) A class III myosin expressed in the retina is a potential candidate for Bardet-Biedl syndrome, *Genomics 79*, 621−624.
7. Dosé, A. C., Hillman, D. W., Wong, C., Sohlberg, L., Lin-Jones, J., and Burnside, B. (2003) Myo3A, one of two class III myosin genes expressed in vertebrate retina, is localized to the calycal processes of rod and cone photoreceptors and is expressed in the sacculus, *Mol. Biol. Cell 14*, 1058−1073.
8. Dosé, A.C., Lin-Jones, J., and Burnside, B. (2004) In *Cell Biology and Disease of the Outer Retina* (Williams, D. S., Ed.) pp 133−162.
9. Dalal, J. S., Dosé, A. C., Burnside, B., and Battelle, B-A. (2005) Developmental expression of myo3b in mouse retina, *Invest. Ophthalmol. Visual Sci. S46*, eAbstract 3964.
10. Hicks, J. L., and Williams, D. S. (1992) Distribution of the myosin I-like NINAC proteins in the *Drosophila* retina and ultrastructural analysis of mutant phenotypes, *J. Cell Sci. 101*, 247−254.
11. Li, H. S., Porter, J. A., and Montell, C. (1998) Requirement for the NINAC kinase/myosin for stable termination of the visual cascade, *J. Neurosci. 18*, 9601−9606.
12. Chyb, S., Hevers, W., Forte, M., Wolfgang, W. J., Selinger, Z., and Hardie, R. C. (1999) Modulation of the light response by cAMP in *Drosophila* photoreceptors, *J. Neurosci. 19*, 8799−8807.
13. Porter, J. A., Yu, M., Doberstein, S. K., Pollard, T. D., and Montell, C. (1993) Dependence of calmodulin localization in the retina on the NINAC unconventional myosin, *Science 262*, 1038−1042.
14. Hofstee, C. A., Henderson, S., Hardie, R. C., and Stavenga, D. G. (1996) Differential effects of NINAC proteins (p132 and p174) on light-activated currents and pupil mechanism in *Drosophila* photoreceptors, *Visual Neurosci.* 897−906.
15. Cronin, M. A., Diao, F., and Tsunoda, S. (2004) Light-dependent subcellular translocation of $G_q$alpha in *Drosophila* photoreceptors is facilitated by the photoreceptor-specific myosin III NINAC, *J. Cell Sci. 117*, 4797−4806.
16. Lee, S. J., and Montell, C. (2004) Light-dependent translocation of visual arrestin regulated by the NINAC myosin III, *Neuron 43*, 95−103.
17. Satoh, A. K., and Ready, D. F. (2005) Arrestin 1 mediated light-dependent rhodopsin endocytosis and cell survival. *Curr. Biol. 15*, 1722−1733.
18. Walsh, T., Walsh, V., Vreugde, S., Hertzano, R., Shahin, H., Haika, S., Lee, M. K., Kanaan, M., King, M., and Avraham, K. B. (2002) From flies' eyes to our ears: mutations in a human class III myosin cause progressive nonsyndromic hearing loss DFNB30, *Proc. Natl. Acad. Sci. U.S.A. 99*, 7518−7523.
19. Schneider, M. E., Dosé, A. C., Salles, F. T., Chang, W., Erickson, F. L., Burnside, B., and Kachar, B. (2006) A new compartment at stereocilia tips defined by spatial and temporal patterns of myosin IIIa expression, *J. Neurosci. 26*, 10243−10252.
20. Edwards, S. C., and Battelle, B. A. (1987) Octopamine- and cyclic AMP-stimulated phosphorylation of a protein in *Limulus* ventral and lateral eyes, *J. Neurosci. 7*, 2811−2820.
21. Edwards, S. C., Andrews, A. W., Renninger, G. H., Wiebe, E. M., and Battelle, B-A. (1990) Efferent innervation to *Limulus* eyes *in vivo* phosphorylates a 122 kD protein, *Biol. Bull. 178*, 267−278.
22. Battelle, B-A. (2002) Circadian efferent input to *Limulus* eyes: anatomy, circuitry, and impact, *Microsc. Res. Tech. 58*, 345−355.
23. Chamberlain, S. C., and Barlow, R. B., Jr. (1984) Transient membrane shedding in *Limulus* photoreceptors: control mechanisms under natural lighting, *J. Neurosci. 4*, 2792−2810.
24. Chamberlain, S. C., and Barlow, R. B., Jr. (1979) Light and efferent activity control rhabdom turnover in *Limulus* photoreceptors, *Science 206*, 361−363.
25. Kier, C. K., and Chamberlain, S. C. (1990) Dual controls for screening pigment movement in photoreceptors of the *Limulus* lateral eye: circadian efferent input and light, *Visual Neurosci. 4*, 237−255.

26. Furch, M., Fujita-Becker, S., Geeves, M. A., Holmes, K. C., and Manstein, D. J. (1999) Role of the salt-bridge between switch-1 and switch-2 of *Dictyostelium* myosin, *J. Mol. Biol. 290*, 797−809.
27. Onishi, H., Kojima, S-I., Katoh, K., Fujiwara, K., Martinez, H. M., and Morales, M. F. (1998) Functional transitions in myosin: Formation of a critical salt-bridge and transmission of effect to the sensitive tryptophan, *Proc. Natl. Acad. Sci. U.S.A. 95*, 6653−6658.
28. Sineshchekova, O. O., Cardasis, H. L., Severance, E. G., Smith, W. C., and Battelle, B-A. (2004) Sequential phosphorylation of visual arrestin in intact *Limulus* photoreceptors: identification of a highly light-regulated site, *Visual Neurosci. 21*, 715−724.
29. Wang, F., Harvey, E. V., Conti, M. A., Wei, D., and Sellers, J. R. (2000) A conserved negatively charged amino acid modulates function in human nonmuscle myosin IIA, *Biochemistry 39*, 5555−5560.
30. Laemmli, U. K. (1970) Cleavage of structural proteins during the assembly of the head of bacteriophage T4, *Nature 227*, 680−685.
31. Klee, C. B. (1977) Conformational transition accompanying the binding of Ca^{2+} to the protein activator of 3′,5′-cyclic adenosine monophosphate phosphodiesterase, *Biochemistry 16*, 1017−1024.
32. Casnellie, J. E. (1991) Assay of protein kinases using peptides with basic residues for phosphocellulose binding, *Methods Enzymol. 200*, 115−120.
33. Kass, L., and Renninger, G. H. (1988) Circadian change in function of *Limulus* ventral photoreceptors, *Visual Neurosci. 1*, 3−11.
34. Warren, M. K., and Pierce, S. K. (1982) Cell-volume regulatory systems in the *Limulus* myocardium—an interaction of ions and quaternary ammonium-compounds, *Biol. Bull. 163*, 504−516.
35. Seamon, K. B., Padgett, W., and Daly, J. W. (1981) Forskolin: unique diterpene activator of adenylate cyclase in membranes and in intact cells, *Proc. Natl. Acad. Sci. U.S.A. 78*, 3363−3367.
36. O'Reilly, D.R., Miller, L.K., and Luckow, V.A. (1994) *Baculovirus Expression Vectors*, A Laboratory Manual, Oxford University Press, New York.
37. Battelle, B. A., Dabdoub, A., Malone, M. A., Andrews, A. W., Cacciatore, C., Calman, B. G., Smith, W. C., and Payne, R. (2001) Immunocytochemical localization of opsin, visual arrestin, myosin III, and calmodulin in *Limulus* lateral eye retinular cells and ventral photoreceptors, *J. Comp. Neurol. 435*, 211−225.
38. Glass, D. B., Cheng, H. C., Mende-Mueller, L., Reed, J., and Walsh, D. A. (1989) Primary structural determinants essential for potent inhibition of cAMP-dependent protein kinase by inhibitory peptides corresponding to the active portion of the heat-stable inhibitor protein, *J. Biol. Chem. 264*, 8802−8810.
39. Chakravarthy, B. R., Bussey, A., Whitfield, J. F., Sikorska, M., Williams, R. E., and Durkin, J. P. (1991) The direct measurement of protein kinase C (PKC) activity in isolated membranes using a selective peptide substrate, *Anal. Biochem. 196*, 144−150.
40. Hashimoto, Y., and Soderling, T. R. (1987) Calcium calmodulin-dependent protein kinase II and calcium phospholipid-dependent protein kinase activities in rat tissues assayed with a synthetic peptide, *Arch. Biochem. Biophys. 252*, 418−425.
41. Marin, O., Meggio, F., and Pinna, L. A. (1994) Design and synthesis of two new peptide substrates for the specific and sensitive monitoring of casein kinases-1 and -2, *Biochem. Biophys. Res. Commun. 198*, 898−905.
42. Battelle, B. A., Andrews, A. W., Kempler, K. E., Edwards, S. C., and Smith, W. C. (2000) Visual arrestin in *Limulus* is phosphorylated at multiple sites in the light and in the dark, *Visual Neurosci. 17*, 813−822.
43. Boyle, W. J., van der Geer, P., and Hunter, T. (1991) Phosphopeptide mapping and phosphoamino acid analysis by two-dimensional separation on thin-layer cellulose plates, *Methods Enzymol. 201*, 110−149.
44. Spudich, J. A., and Watt, S. (1971) The regulation of rabbit skeletal muscle contraction. I, biochemical studies of the interaction of the tropomyosin-troponin complex with actin and the proteolytic fragments of myosin, *J. Biol. Chem. 246*, 4866−4871.
45. Trentham, D. R., Bardsley, R. G., Eccleston, J. F., and Weeds, A. G. (1972) Elementary processes of the magnesium ion-dependent adenosine triphosphatase activity of heavy meromyosin. A transient kinetic approach to the study of kinases and adenosine triphosphatases and a colorimetric inorganic phosphate assay *in situ*, *Biochem. J. 126*, 635−644.
46. Weeds, A. G., and Taylor, R. S. (1975) Separation of subfragment-1 isoenzymes from rabbit skeletal muscle myosin, *Nature 257*, 54−56.
47. Milligan, R. A. (1996) Protein-protein interactions in the rigor actomyosin complex, *Proc. Natl. Acad. Sci. U.S.A. 93*, 21−26.
48. Chijiwa, T., Mishima, A., Hagiwara, M., Sano, M., Hayashi, K., Inoue, T., Naito, K., Toshioka, T., and Hidaka, H. (1990) Inhibition of forskolin-induced neurite outgrowth and protein phosphorylation by a newly synthesized selective inhibitor of cyclic amp-dependent protein kinase, N-[2-(p-bromocinnamylamino)ethyl]-5-isoquinolinesulfonamide (H-89), of PC12D Pheochromocytoma cells, *J. Biol. Chem. 265*, 5267−5272.
49. Huang, Y. Y., Martin, K. C., and Kandel, E. R. (2000) Both protein kinase A and mitogen-activated protein kinase are required in the amygdala for the macromolecular synthesis-dependent late phase of long-term potentiation, *J. Neurosci. 20*, 6317−6325.
50. House, C., and Kemp, B. E. (1987) Protein kinase C contains a pseudosubstrate prototope in its regulatory domain, *Science 238*, 1726−1728.
51. Malinow, R., Schulman, H., and Tsien, R. W. (1989) Inhibition of postsynaptic PKC or CaMKII blocks induction but not expression of LTP, *Science 245*, 862−866.
52. Kobayashi, E., Nakano, H., Morimoto, M., and Tamaoki, T. (1989) Calphostin C (UCN-1028C), a novel microbial compound, is a highly potent and specific inhibitor of protein kinase C, *Biochem. Biophys. Res. Commun. 159*, 548−553.
53. Davies, S. P., Reddy, H., Caivano, M., and Cohen, P. (2000) Specificity and mechanism of action of some commonly used protein kinase inhibitors, *Biochem. J. 351*, 95−105.
54. Biemann, K. (1992) Mass spectrometry of peptides and proteins, *Annu. Rev. Biochem. 61*, 977−1010.
55. Edwards, S. C., Wishart, A. C., Wiebe, E. M., and Battelle, B. A. (1989) Light-regulated proteins in *Limulus* ventral photoreceptor cells, *Visual Neurosci. 3*, 95−105.
56. Minke, B., Rubinstein, C. T., Sahly, I., Bar-Nachum, S., Timberg, R., and Selinger, Z. (1990) Phorbol ester induces photoreceptor-specific degeneration in a *Drosophila* mutant, *Proc. Natl. Acad. Sci. U.S.A. 87*, 113−117.
57. Smith, D. P., Ranganathan, R., Hardy, R. W., Marx, J., Tsuchida, T., and Zuker, C. S. (1991) Photoreceptor deactivation and retinal degeneration mediated by a photoreceptor-specific protein kinase C, *Science 254*, 1478−1484.
58. Furch, M., Geeves, M. A., and Manstein, D. J. (1998) Modulation of actin affinity and actomyosin adenosine triphosphatase by charge changes in the myosin motor domain, *Biochemistry 37*, 6317−6326.
59. Yengo, C. M., and Sweeney, H. L. (2004) Functional role of loop 2 in myosin V, *Biochemistry 43*, 2605−2612.
60. Sellers, J. R. (1999) *Myosins*, 2nd ed., Oxford University Press, New York.
61. Nalavadi, V., Nyitrai, M., Bertolini, C., Adamek, N., Geeves, M. A., and Bähler, M. (2005) Kinetic mechanisms of myosin IXB and the contributions of two class IX-specific regions, *J. Biol. Chem. 280*, 38957−38968.
62. Ng, K. P., Kambara, T., Matsuura, M., Burke, M., and Ikebe, M. (1996) Identification of myosin III as a protein kinase, *Biochemistry 35*, 9392−9399.
63. Komaba, S., Inoue, A., Maruta, S., Hosoya, H., and Ikebe, M. (2003) Determination of human myosin III as a motor protein having a protein kinase activity, *J. Biol. Chem. 278*, 21352−21360.
64. Dosé, A. C., Ananthanarayanan, S., Moore, J. E., Burnside, M. B., and Yengo, C. M. (2007) Kinetic mechanism of human myosin IIIA, *J. Biol. Chem. 282*, 216−31.
65. Kambara, T., Komaba, S. and Ikebe, M. (2006) Human myosin III is a motor having an extremely high affinity for actin, *J. Biol. Chem. 281*, 37291−37301.
66. Hicks, J. L., Liu, X., and Williams, D. S. (1996) Role of the NINAC proteins in photoreceptor cell structure: ultrastructure of *nina*C deletion mutants and binding to actin filaments, *Cell Motil. Cytoskeleton 35*, 367−379.
67. Sacunas, R. B., Papuga, M. O., Malone, M. A., Pearson, A. C., Jr., Marjanovic, M., Stroope, D. G., Weiner, W. W., Chamberlain, S. C., and Battelle, B.-A. (2002) Multiple mechanisms of rhabdom shedding in the lateral eye of *Limulus polyphemus*, *J. Comp. Neurol. 449*, 26−42.
68. Runyon, S. L., Washicosky, K. J., Brenneman, R. J., Kelly, J. R., Khadilkar, R. V., Heacock, K. F., McCormick, S. M., Williams, K. E., and Jinks, R. N. (2004) Central regulation of photosensitive

membrane turnover in the lateral eye of *Limulus*, II: Octopamine acts via adenylate cyclase/cAMP-dependent protein kinase to prime the retina for transient rhabdom shedding, *Visual Neurosci. 21*, 749−763.
69. Jinks, R. N., White, R. H., and Chamberlain, S. C. (1996) Dawn, diacylglycerol, calcium, and protein kinase C−the retinal wrecking crew. A signal transduction cascade for rhabdom shedding in the *Limulus* eye, *J. Photochem. Photobiol. B 35*, 45−52.
70. Dabdoub, A., Jinks, R. N., Wang, Y., Battelle, B. A., and Payne, R. (2003) Desensitization of the photoresponse in *Limulus* ventral photoreceptors by protein kinase C precedes rhabdomere disorganization and endocytosis, *Visual Neurosci. 20*, 241−248.
71. White, R. H., Seifert, P., and Bennett, R. R. (1992) Phorbol ester mimics ultrastructural effects of light in photoreceptors of *Manduca* rhabdomere disorganization and assembly, *Invest. Ophthalmol. Visual Sci. 33*, 739.
72. Blest, A. D., Stowe, S., Carter, M., and Tsukitani, Y. (1992) Manipulation of phototransductive membrane turnover by crab photoreceptors *in vitro:* effects of two protein kinase activators, SC-9 and phorbol ester in the presence of a protein phosphatase inhibitor, okadaic acid, *J. Comp. Physiol. [A] 170*, 189−199.
73. Blest, A. D., Stowe, S., And, Delaney, A. (1994) An inhibitor of diacylglycerol-activated protein-kinase Cs blocks the effects of a diacylglycerol lipase inhibitor, U-57908, on the light-dependent renewal of crab rhabdoms *in vitro*, *J. Comp. Physiol. [A] 175*, 611−617.
74. Porter, J. A., and Montell, C. (1993) Distinct Roles of the Drosophila ninaC kinase and myosin domains revealed by systematic mutagenesis, *J. Cell Biol. 1993*, 601−612.

BI062112U